Deformation of a conducting drop in a randomly fluctuating electric field

Rajarshi Sengupta, Lynn M. Walker, and Aditya S. Khair*
Department of Chemical Engineering, Carnegie Mellon University, Pittsburgh, Pennsylvania 15213, USA

(Received 12 December 2019; accepted 27 May 2020; published 9 June 2020)

We quantify the transient deformation and breakup of a conducting drop suspended in a dielectric medium and subjected to a fluctuating electric field. Specifically, the magnitude of the field fluctuates randomly in time, while its orientation is fixed. Hence, the deformation of the drop is axisymmetric about the direction of the field. The temporal fluctuations are described by a stationary Markovian Gaussian process, characterized by a mean, variance, and correlation time. Small deformation theory predicts that the fluctuations produce a larger deformation than under a steady electric field of strength equal to the mean of the fluctuating electric field. Next, we utilize boundary integral computations to quantify the deformation and breakup of drops beyond the small deformation regime. When the mean of the fluctuating field is greater than the critical field for breakup under a steady field, we find that the average time taken to undergo breakup is less than that under an equivalent steady field. More interestingly, a certain fraction of drops are observed to undergo breakup even when the mean field is less than the critical field. The fraction of drops undergoing breakup and the range of mean electric field below the critical where breakup is observed depends on the strength of fluctuations of the electric field. An operating map is presented for the percentage of drops undergoing breakup as a function of the dimensionless mean field for different strength of field fluctuations. The present study sheds light on the response of drops in applications such as electrocoalescence and electroemulsification, where interactions with surrounding drops or disturbances in operating conditions can produce a random field around a drop, even when the applied macroscopic field is uniform.

DOI: 10.1103/PhysRevFluids.5.063701

I. INTRODUCTION

When an electric field is applied around a drop of fluid of initial radius a_0, suspended in another immiscible fluid, there is a discontinuity in the electric field distribution across the interface due to a mismatch in the electrical properties of the two fluids. As a result, electric stresses are generated at the interface, which deform the drop from an initial spherical shape. The electric stresses are balanced by the capillary stress, which arise due to an interfacial tension, γ. For perfectly conducting or perfectly dielectric drops suspended in a perfectly dielectric liquid, the electric stresses are nonuniform along the interface, and consequently the drop deforms along the direction of the applied field into a prolate shape [1–7]. Understanding how drops respond to an applied electric field is important in applications like electrospray mass spectrometry [8], electrocoalescence [9,10], and electric-field-based emulsification [11,12]. For small values of a uniform, direct current (D.C.) applied electric field, the deformation of the drop is small. In this small deformation limit, Allan and Mason [5] predicted that the steady deformation of a conducting drop in a dielectric liquid,

*akhair@andrew.cmu.edu

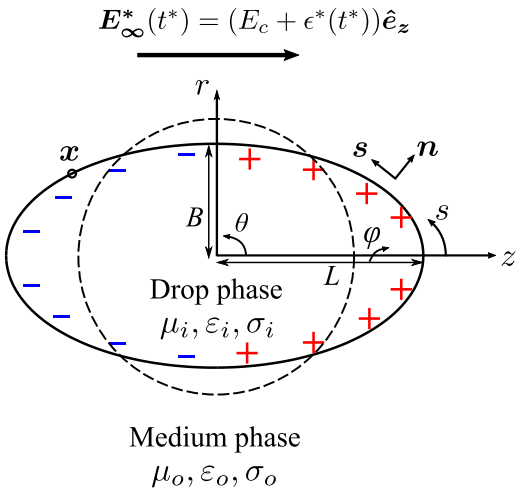

FIG. 1. Schematic of the electric field induced deformation of a conducting drop. The axis of symmetry, φ, is along the direction of the electric field, E^*_∞. The average magnitude of the electric field is E_c, and the fluctuations are denoted by ϵ^*. The drop having viscosity μ_i, permittivity ε_i and conductivity σ_i is suspended in a dielectric medium with viscosity μ_o, permittivity ε_o and conductivity σ_o. The initially undeformed state of the drop is shown by the dashed curve. The semi-major and semiminor axis of the deformed drop are denoted by L and B, respectively. The unit normal ($\boldsymbol{n}$) and tangential ($\boldsymbol{s}$) vectors, the continuous tangential coordinate (s), the polar angle (θ), and a fixed source point on the interface ($\boldsymbol{x}$) are also shown.

$\mathcal{D} = \frac{L-B}{L+B}$, is proportional to the square of the applied electric field, E^*_∞,

$$\mathcal{D} \sim \tfrac{9}{16}\mathrm{Ca}_E, \tag{1}$$

as $\mathrm{Ca}_E \to 0$. Here L and B are the half lengths of the drop along and normal to the direction of the applied electric field, respectively (Fig. 1), and $\mathrm{Ca}_E = a_0\varepsilon_o E^{*2}_\infty/\gamma$ is the electric capillary number defined as the ratio of electric stresses to capillary stress, with ε_o representing the dielectric constant of the medium phase fluid. The electric capillary number can also be defined as the ratio of the capillary time scale, $t_c = \mu_o a_0/\gamma$, which is the time scale for the capillary stress to restore the drop to the undeformed state, to the flow time scale, $t_f = a_0/U$, where the velocity scale, $U = \varepsilon_o a_0 E^{*2}_\infty/\mu_o$, is obtained by balancing the viscous shear to electric stresses, with μ_o denoting the viscosity of the medium phase fluid. To $\mathcal{O}(\mathrm{Ca}_E)$, the drop deforms to a spheroidal shape. Equation 1 is first order in Ca_E; the deformation is nonlinear in Ca_E at larger values of the electric field strength.

The small deformation theory given by Eq. (1) is valid for $\mathrm{Ca}_E \ll 1$. At larger field strengths, the drop deformation is nonlinear in Ca_E, and the shape is nonspheroidal [13–15]. The inclusion of higher order terms to (1) is not sufficient to predict the experimentally observed deformation [16]. The drop ultimately breaks up to form smaller drops beyond a critical value of the electric field. Numerical methods, particularly the boundary integral method and the finite element method, have been employed to calculate the steady nonlinear deformation of drops at larger Ca_E, and predict the breakup criteria and breakup modes for both uniform [17–22] and oscillatory [13] external fields. The manner in which the deformed state is attained, i.e., the transient deformation of the drop, has also been established [23–26].

Previous studies have predominantly focused on the transient deformation and breakup of a single drop subjected to a deterministic (uniform or oscillatory) external electric field. In practical

systems, the response of a drop will be influenced by the interaction with surrounding drops, interaction with walls, and disturbances in operating conditions. For instance, in equipment like electrocoalescers or electroemulsifiers, the surrounding drops will have different sizes and be randomly distributed around a given ("test") drop. Thus, even when the applied macroscopic voltage (for example, the potential difference across the electrodes in an electrocoalescer) is steady, the behavior of the test drop could be drastically different from the response of a single drop under a deterministic field. An equivalent description of the dynamics of drop deformation and breakup in such practical applications is to quantify drop response to a randomly fluctuating external field. A similar approach has been adopted to study drop fragmentation in mixers and packed beds via experiments [27–29], and simulations [29–32]. In particular, the fluid flow through a dilute fixed bed was modeled as an equivalent anisotropic Gaussian flow field through a spectral expansion method, where the wave number vectors were chosen from statistical distributions to realize a desired flow field. The orientation of tracer polymers, extension of polymer molecules, and droplet breakup in the simulated stochastic flow field was predicted [29–32]. An alternate approach to model a stochastic external flow field was followed in Ref. [33], where the random component of the flow was modeled as an Ornstein-Uhlenbeck process using a mean, variance, and correlation time. The response of the drop was quantified in terms of a probability distribution function of the final deformation and breakup.

However, to the best of our knowledge, the dynamics of drop deformation and breakup in a random electric field has not been studied before. Therefore, in this work, we quantify the transient deformation and breakup of a drop of conducting liquid suspended in a dielectric liquid when subjected to an electric field, the magnitude of which fluctuates randomly in time. We choose the simplest system of a conducting drop, where no sustained fluid flow exists at steady state, to elucidate how fluctuations affect deformation and the criterion for breakup. Again, we emphasize the importance of this problem in the context of practical applications like electrocoalescence and electroemulsification. A complete description would have to account for many-body hydrodynamic and electrostatic interactions between drops, and spatial fluctuations in the electric field. Nevertheless, our approach is a reasonable first step. We employ small deformation theory and the boundary integral method to predict the effect of fluctuations on the final state of the drop. In Sec. II, we state the problem and describe the statistics of the electric field signal. We also outline the small deformation theory, boundary integral method formulation, and the numerical scheme used to implement the computations. In Sec. III we present the results of the theory and computations. In Sec. IV we discuss the results, and draw an analogy with the extension and coil-stretch transition of polymers in flow fields. Finally, we state the conclusions in Sec. V.

II. MODELING DROP DEFORMATION AND BREAKUP

An uncharged drop of a conducting liquid with initial radius a_0 is suspended in a dielectric medium, as shown in Fig. 1. The drop and medium phase fluids are density and viscosity matched. The drop is subjected to an electric field, the magnitude of which fluctuates randomly in time, but the direction remains fixed. The electric field deforms the drop from its initial, spherical state. We assume that the deformation is axisymmetric and quantify the effect of fluctuations in the electric field on the transient deformation and criteria for drop breakup. The problem requires the calculation of electric field distribution and fluid flow in the drop and medium phase fluids. Although at steady state there is no fluid flow for conducting drops, the solution to the flow problem is necessary to predict the transient deformation of the drop. We present the governing equations in this section. Henceforth, a superscript "*" denotes a dimensional variable, and a lack of the superscript denotes a physical parameter, scale, dimensionless group, or the dimensionless version of a dimensional variable.

A. Statistics of the fluctuating electric field

The external electric field, $\boldsymbol{E}^*_\infty$, is composed of a constant part, E_c, and a part whose magnitude fluctuates randomly in time, ϵ^*, i.e., $\boldsymbol{E}^*_\infty(t^*) = [E_c + \epsilon^*(t^*)]\hat{\boldsymbol{e}}_z$, where $\hat{\boldsymbol{e}}_z$ is the unit vector along the direction of the field. In practice, the fluctuations could be caused by the polydispersity of the system, interaction with surrounding drops, interaction of the drop with walls, or disturbances in operating conditions. Note that we only consider temporal fluctuations of the field and neglect spatial stochasticity. This assumption is valid when the source of the fluctuations is solely temporal disturbances in operating conditions, or when the concentration of drops in the system is relatively dilute, such that the center-to-center distance between drops is much larger than their radius, and drops do not reorient or experience relative motion due to electrostatic interactions [34]. Instead of determining the contribution of each of the possible factors to the fluctuations in the field, we assume that the random temporal variation of the electric field is described by a stationary Markovian Gaussian process (the Ornstein-Uhlenbeck process) [33,35]. Hence, the evolution of ϵ^* follows the stochastic differential equation

$$\frac{d\epsilon^*}{dt^*} = -\lambda^*[\epsilon^* - g^*_w(t^*)], \tag{2}$$

where g^*_w is the underlying Gaussian white noise driving the fluctuations and λ^* is the inverse correlation time. The fluctuations in the electric field are specified by λ^* and the statistics of g^*_w. We nondimensionalize Eq. (2) using E_c to scale the electric field, and the capillary time, $t_c = \mu_o a_0/\gamma$, to scale time, and obtain the dimensionless governing equation for the fluctuations in electric field as

$$\frac{d\epsilon}{dt} = -\lambda[\epsilon - g_w(t)]. \tag{3}$$

Here, $\lambda = \lambda^* t_c$ is the dimensionless inverse correlation time. The underlying Gaussian white noise has the properties $\langle g_w(t)\rangle = 0$, and $\langle g_w(t) g_w(t')\rangle = 2G_w\delta(t - t')$, where δ is the Dirac δ function, and $2G_w$ is the variance of the white noise. A term in the angle brackets denotes an average over an ensemble of initial distribution of the variable. The driven noise is generated using an algorithm described in Ref. [35], after integrating Eq. (3) to obtain

$$\epsilon(t) = \epsilon_0 e^{-\lambda t} + \int_0^t \lambda e^{-\lambda(t-t')} g_w(t')\, dt', \tag{4}$$

where ϵ_0 is an initial value of the fluctuation. At any given time, the driven noise is Gaussian distributed, $\epsilon(t) \sim \mathcal{N}(\langle\epsilon_0\rangle e^{-\lambda t}, G_w\lambda)$, where $\mathcal{N}(\overline{\mu}, \nu)$ denotes a normal distribution with mean $\overline{\mu}$ and variance ν. The distribution of initial value of the fluctuations, ϵ_0, is given by

$$\mathcal{P}(\epsilon_0) = \frac{1}{\sqrt{2\pi G_w\lambda}} \exp\left\{-\frac{(\epsilon_0 - \langle\epsilon_0\rangle)^2}{2G_w\lambda}\right\}. \tag{5}$$

We choose $\langle\epsilon_0\rangle = 0$, so that the mean electric field is set by the constant part, E_c, and fluctuations to the field is set by the variance of $\epsilon(t)$, i.e., $G_w\lambda$. The driven noise has the properties

$$\langle\epsilon(t)\rangle = 0, \tag{6}$$

$$\langle\epsilon(t)\epsilon(t')\rangle = G_w\lambda \exp(-\lambda|t - t'|). \tag{7}$$

where the term $\langle ...\rangle$ denotes an average over an ensemble of initial distribution of ϵ_0, given by Eq. (5).

It follows from Eq. (7) that $\epsilon(t)$ is an exponentially correlated colored noise. Further, the nondimensional electric field follows a Gaussian distribution at any given time, $E_\infty \sim \mathcal{N}(1, G_w\lambda)$. A simulated fluctuating electric field signal is shown in Fig. 2(a) for a specified variance, $G_w\lambda = 0.1$. The signal was obtained by taking an average over 100 realizations of the algorithm over the initial

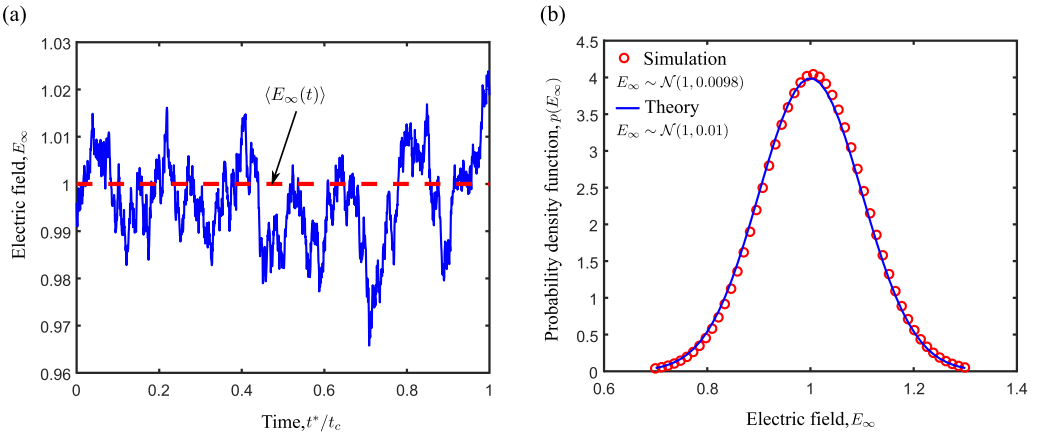

FIG. 2. (a) A simulated electric field with variance $G_w\lambda = 0.1$. The solid line is an average over 100 realizations of the algorithm over the initial distribution of ϵ_0. The dashed line shows the mean value of the fluctuations. (b) Probability density function of the numerically computed (circles) and theoretically predicted (solid line) electric field at $t = 1$.

distribution given by Eq. (5). Comparing the statistics of the simulated signal with the statistics predicted theoretically, i.e., $E_\infty \sim \mathcal{N}(1, G_w\lambda)$ at $t = 1$, shows that averaging over 100 realizations over Eq. (5) is sufficient to describe the fluctuating electric field [Fig. 2(b)]. The random temporal fluctuations can be generated in experiments by using virtual instrumentation platforms such as Labview to trigger the voltage source. The waveform of the voltage to be applied can be specified in the virtual instrumentation.

B. Small deformation theory

We first consider a slightly spheroidal deformation of the drop surface at small values of the mean electric field (which corresponds to a small value of the mean electrical capillary number). In this limit, the drop can be treated as a sphere during the implementation of the boundary conditions [25,26]. Spherical coordinates are employed and the axis of symmetry is taken along the direction of the applied field. The electric field is irrotational, and since the drop is electrically neutral, Gauss's law reduces to the Laplace equation for the inner and outer electrostatic potentials ($\phi^*_{i,o}$), giving

$$\nabla^{*2}\phi^*_{i,o} = 0, \tag{8}$$

with the electric field calculated using $\boldsymbol{E}^*_{i,o} = -\nabla^*\phi^*_{i,o}$. The potential in the drop phase, ϕ^*_i is bounded at the center of the drop, and at far field, the potential in the medium phase satisfies $-\nabla^*\phi^*_o \to \boldsymbol{E}^*_\infty$. The electric field distribution in the drop and medium is obtained from the solution of Eq. (8) with these boundary conditions, along with the interface conditions at the surface of the drop, $r^* = a_0$, where the potential is continuous,

$$\phi^*_i = \phi^*_o, \tag{9}$$

and the jump in electric displacement follows

$$[-\varepsilon\nabla^*\phi^*\cdot\boldsymbol{n}] = q^*(t^*). \tag{10}$$

The term in the square brackets in Eq. (10) represents a difference between inner and outer quantities, $\boldsymbol{n}$ is a unit normal vector, positive in the outward direction (Fig. 1), and q^* is the interfacial charge density, which is an unknown. Hence, an additional interface condition to describe the continuity of current across the interface is used. For a perfectly conducting drop, effects of surface

charge convection and charge relaxation can be neglected, and the interfacial charge conservation equation reduces to [7,36]

$$[\sigma \nabla^* \phi^* \cdot \boldsymbol{n}] = 0. \tag{11}$$

For a perfectly conducting drop, $\sigma_i \gg \sigma_o$, hence Eq. (11) predicts that the normal electric field inside the drop phase, $E_{n,i} = 0$.

After solving the electric field distribution in the two phases, the Maxwell electric stresses at the interface can be calculated using $\boldsymbol{\tau}^*_{E_{i,o}} = \varepsilon_{i,o} \boldsymbol{E}^*_{i,o} \boldsymbol{E}^*_{i,o} - (\boldsymbol{E}^*_{i,o} \cdot \boldsymbol{E}^*_{i,o}) \boldsymbol{I}/2$.

The flow field in the drop and medium phases is governed by the continuity equation and the Navier-Stokes equation,

$$\nabla^* \cdot \boldsymbol{u}^*_{i,o} = 0, \tag{12}$$

and

$$\rho_{i,o} \left[\frac{\partial \boldsymbol{u}^*_{i,o}}{\partial t^*} + \boldsymbol{u}^*_{i,o} \cdot \nabla^* \boldsymbol{u}^*_{i,o} \right] = -\nabla^* p^*_{i,o} + \mu_{i,o} \nabla^{*^2} \boldsymbol{u}^*_{i,o}, \tag{13}$$

where $\boldsymbol{u}$ is the velocity and p is the hydrostatic pressure. We consider millimeter sized drops in this work. Hence, even though the electric field is fluctuating randomly in time, the flow field is described by the deterministic Navier-Stokes equations. For microscale drops, fluctuations driven by thermal noise may lead to deformation of the drop interface and would necessitate a description of the flow field using fluctuating hydrodynamics, where a stochastic forcing term is added to the momentum balance Eq. (13) [37,38]. How such thermal fluctuations couple with a deformation due to an applied field is an interesting problem for future study.

We first nondimensionalize the problem. The electric field is scaled with the constant mean electric field, E_c. Distance is scaled with the radius of the underformed drop, a_0. The capillary time, t_c, is used to normalize time. Interfacial charge density is rendered dimensionless using $\varepsilon_o E_c$. Electric stresses ($\varepsilon_o E_c^2$) are chosen to scale stresses. The scale for velocity is obtained by balancing electric stresses and viscous stress at the interface, giving $U = \varepsilon_o E_c^2 a_0/\mu_o$. These scalings lead to the dimensionless momentum balance,

$$\frac{\mathrm{Re}_{i,o}}{\langle \mathrm{Ca}_E \rangle} \frac{\partial \boldsymbol{u_{i,o}}}{\partial t} + \mathrm{Re}_{i,o} \boldsymbol{u}_{i,o} \cdot \nabla \boldsymbol{u}_{i,o} = -\nabla p_{i,o} + \nabla^2 \boldsymbol{u_{i,o}}, \tag{14}$$

where $\mathrm{Re}_{i,o} = \rho_{i,o} \varepsilon_o E_c^2 a_0^2/\mu_{i,o}^2$ is the Reynolds number, and $\langle \mathrm{Ca}_E \rangle = a_0 \varepsilon_o E_c^2/\gamma$ is the mean electric capillary number. We assume creeping flow, $\mathrm{Re}_{i,o} \ll 1$, and further assume that $\mathrm{Re}_{i,o}/\langle \mathrm{Ca}_E \rangle \ll 1$ to reduce the momentum balance to

$$-\nabla p_{i,o} + \nabla^2 \boldsymbol{u_{i,o}} = 0. \tag{15}$$

Since the problem is axisymmetric, Eq. (15) can be solved using a stream function ψ, which automatically satisfies incompressibility Eq. (12). The stream function satisfies the biharmonic equation

$$D^4 \psi_{i,o} = 0, \tag{16}$$

where $D^4 = D^2(D^2)$, and $D^2 = \partial^2/\partial r^2 + (\sin\theta/r^2)\{\partial/\partial\theta[(1/\sin\theta)\partial/\partial\theta]\}$. The velocity is related to the stream function through

$$\boldsymbol{u}_{i,o} = \nabla \times \left[\frac{\psi_{i,o}}{r \sin\theta} \hat{\boldsymbol{e}}_{\boldsymbol{\phi}} \right], \tag{17}$$

where $\hat{\boldsymbol{e}}_{\boldsymbol{\phi}}$ is the unit vector in the azimuthal direction. The flow field is subject to the constraints that the velocity at the center of the drop is bounded, and the far field condition in the medium, $\boldsymbol{u}_o = 0$ at $\boldsymbol{r} \to \infty$. The complete solution requires four more interface conditions. At small field

strengths where $\langle \mathrm{Ca}_E \rangle \ll 1$, the interface is only slightly deformed, and the instantaneous shape can be described using [25,26]

$$\xi = 1 + \tfrac{2}{3}\mathcal{D}(t)(3\cos^2\theta - 1), \tag{18}$$

where $\mathcal{D}(t)$ is the instantaneous deformation of the drop, defined as the ratio of the difference in semimajor and semiminor axis of the drop to the sum of the semimajor and semiminor axis. In the limit of small deformation ($\langle \mathrm{Ca}_E \rangle \ll 1$), the interface conditions

$$u_{\theta,i} = u_{\theta,o} \tag{19}$$

and

$$u_{r,i} = u_{r,o} = \frac{1}{\langle \mathrm{Ca}_E \rangle}\frac{d\xi}{dt} \tag{20}$$

can be applied at $r = 1$, and the deformation subsequently calculated using the interfacial stress balance equation, which in the absence of surfactant reads

$$(p_i - p_o)\boldsymbol{n} + (\boldsymbol{\tau}_{H,o} - M\boldsymbol{\tau}_{H,i})\cdot\boldsymbol{n} + \left[\boldsymbol{\tau}_{E_{i,o}}\cdot\boldsymbol{n}\right] = \frac{1}{\langle \mathrm{Ca}_E \rangle}(\nabla_s \cdot \boldsymbol{n})\boldsymbol{n}. \tag{21}$$

Here, $\boldsymbol{\tau}_H$ represents the deviatoric stress tensor, and $\nabla_s \cdot \boldsymbol{n}$ is the curvature of the interface where ∇_s is the surface gradient operator, defined as $\nabla_s = (\boldsymbol{I} - \boldsymbol{nn})\cdot\nabla$. A detailed procedure of solution of the equations can be found in Ref. [25], and an overview of the procedure is presented in this work. The general solution of the flow field is obtained from Eqs. (16) and (17), and the constants are rewritten in terms of the instantaneous deformation, $\mathcal{D}$(t) using the constraints of bounded flow at the drop center, far field condition, interfacial velocity Eqs. (19) and (20), and the tangential stress balance obtained from Eq. (21). The normal stress balance is then used to obtain the governing equation for transient deformation,

$$\tau\frac{d\mathcal{D}}{dt} + \mathcal{D} = \mathcal{D}_{\mathrm{DC}}[1 + \epsilon(t)^2], \tag{22}$$

where $\tau = \frac{(19M+16)(2M+3)}{40(M+1)}$, $M = \mu_i/\mu_o$, and $\mathcal{D}_{\mathrm{DC}} = 9\langle \mathrm{Ca}_E \rangle/16$ is the steady deformation of a conducting drop in a dielectric medium under a uniform D.C. electric field at small electric field strengths [5,6]. Integrating Eq. (22), we obtain the instantaneous deformation of a conducting drop in a randomly fluctuating field,

$$\mathcal{D}(t) = \mathcal{D}_{\mathrm{DC}}(1 - e^{-t/\tau}) + \frac{\mathcal{D}_{\mathrm{DC}}}{\tau}\int_0^t [2\epsilon(t')e^{-(t-t')/\tau} + \epsilon(t')^2 e^{-(t-t')/\tau}]\,dt'. \tag{23}$$

The first term on the right-hand side is the expression of the transient deformation of a drop under a uniform D.C. field when transient fluid inertia can be neglected, i.e., the flow is established instantaneously on the timescale that momentum diffuses from the deforming interface [23,25,26]. This predicts that the deformation monotonically settles toward the steady-state result given in Eq. (1) as $t \to \infty$. The second term represents the contribution of the fluctuations in the electric field to the transient deformation. Note that fluctuations lead to $\mathcal{D}(t)$ being nonlocal in time; the history of the electric field is remembered through the correlation time. A closed form solution of $\mathcal{D}(t)$ cannot be obtained because a closed form expression of $\epsilon(t)$ is not known. Therefore, we obtain the statistics (mean and variance) of the instantaneous deformation as

$$\langle \mathcal{D}(t) \rangle = \mathcal{D}_{\mathrm{DC}}(1 + G_w\lambda)(1 - e^{-t/\tau}) \tag{24}$$

and

$$\mathrm{var}[\mathcal{D}(t)] = \frac{\mathcal{D}_{\mathrm{DC}}^2 G_w\lambda}{\tau}(2 + G_w\lambda)(1 - e^{-2t/\tau}). \tag{25}$$

Clearly, the mean deformation of a drop in a randomly fluctuating field is greater than under a uniform D.C. field when the field strength is small, and the difference in deformation increases with fluctuations in the field ($G_w\lambda$). When the fluctuations vanish, i.e., $G_w\lambda \to 0$, the electric field around the drop assumes the form of a steady D.C. field. In this limit, we find that $\langle \mathcal{D}(t)\rangle = \mathcal{D}_{\rm DC}(1 - e^{-t/\tau})$, and $\mathrm{var}(\langle \mathcal{D}(t)\rangle) = 0$, which is the expected result for drop deformation under a steady electric field that is suddenly applied at $t = 0$.

C. Boundary integral formulation

The nonlinear drop deformation at a larger value of the mean electric field, and possible breakup, is predicted using the boundary integral method. This requires the solution of the electric field and fluid flow at the interface only, thereby reducing the dimensionality of the problem by one, and consequently reducing the computational cost [39–41]. The Laplace Eq. (8) is recast into a nondimensional integral equation at the interface [20,22,42,43],

$$\frac{S-1}{4\pi S}\oint_A \frac{\boldsymbol{r}\cdot\boldsymbol{n}(\boldsymbol{x})}{r^3}E_{n,o}(\boldsymbol{y})dA(\boldsymbol{y}) + \frac{S+1}{2S}E_{n,o}(\boldsymbol{x}) = \boldsymbol{E}_\infty\cdot\boldsymbol{n}(\boldsymbol{x}) - \frac{1}{4\pi S}\oint_A q(\boldsymbol{y})dA(\boldsymbol{y}) + \frac{1}{2S}q(\boldsymbol{x}), \tag{26}$$

where $S = \varepsilon_i/\varepsilon_o$ is the ratio of dielectric constant of the drop to medium phase fluid, $\boldsymbol{r} = \boldsymbol{y} - \boldsymbol{x}$ is the difference between an observer point $\boldsymbol{y}$ that can move along the interface and a fixed source point $\boldsymbol{x}$ on the interface. The integral is taken over the surface area, A of the drop. The normal electric field in the drop phase is calculated using the dimensionless form of Eq. (11), $E_{n,i} = RE_{n,o}$, where $R = \sigma_o/\sigma_i$ is the ratio of electrical conductivity of the medium to drop phase fluid. For a conducting drop in a dielectric, $\sigma_i \gg \sigma_o$, hence $E_{n,i} = 0$; however in the computations, instead of prescribing $E_{n,i} = 0$, we specify a very small value of R ($\approx 10^{-10}$). The interface is initially uncharged, hence the normal electric field can be computed at $t = 0$. The tangential field is obtained by an integral transform of the Laplace equation in terms of the electrostatic potential, ϕ_o [22,43,44],

$$\phi_o(\boldsymbol{x}) = \phi_\infty(\boldsymbol{x}) + \oint_A \frac{1}{4\pi r}[E_{n,o}(\boldsymbol{y}) - E_{n,i}(\boldsymbol{y})]dA(\boldsymbol{y}), \tag{27}$$

and using the relation $E_{t,o} = -\partial\phi_o/\partial s$ and Eq. (9). Here, s is the tangential coordinate measured from $\theta = 0$ (Fig. 1), and $E_{t,o} = \boldsymbol{E}_o\cdot\boldsymbol{t}$. From the distribution of the electric field in the drop and medium, the jump in electric stresses at the interface is calculated, which in nondimensional form reads

$$[\boldsymbol{\tau}_E\cdot\boldsymbol{n}] = \tfrac{1}{2}\left[\left(E_{n,o}^2 - SE_{n,i}^2\right) + (S-1)E_{t,o}^2\right]\boldsymbol{n} + E_{t,o}(E_{n,o} - SE_{n,i})\boldsymbol{t} = \Delta p_E\boldsymbol{n} + qE_{t,o}\boldsymbol{t}. \tag{28}$$

For a conducting drop, $E_t = 0$, and $E_{n,i} = 0$, and Eq. (28) reduces to $[\boldsymbol{\tau}_E\cdot\boldsymbol{n}] = (E_{n,o}^2/2)\,\boldsymbol{n}$.

The Stokes Eqs. (15) can be cast as an integral equation in dimensionless form [45], and when the drop and medium are viscosity matched this yields

$$\boldsymbol{u_o}(\boldsymbol{x}) = -\frac{1}{8\pi}\oint_A \Delta\boldsymbol{f}(\boldsymbol{y})\cdot\boldsymbol{J}(\boldsymbol{y},\boldsymbol{x})dA(\boldsymbol{y}), \tag{29}$$

where $\boldsymbol{J}$ denotes the free-space Green's functions for velocity, and $\Delta\boldsymbol{f}(\boldsymbol{y})$ is the jump in hydrodynamic stresses at the observer points on the interface, calculated using Eq. (21).

After obtaining the electric field and interfacial velocity, the interfacial charge is updated using the dimensionless form of Eq. (10),

$$q = E_{n,o} - SE_{n,i}. \tag{30}$$

Finally, the interface is updated using the dimensionless kinematic condition

$$\frac{d\boldsymbol{x}}{dt} = \langle \mathrm{Ca}_E\rangle\,(\boldsymbol{u_o}\cdot\boldsymbol{n})\boldsymbol{n}. \tag{31}$$

TABLE I. Physical properties of the fluids used. The interfacial tension between the fluids is $\gamma = 17$ mN/m [21]. The drop phase corresponds to system (G10) of Ref. [21]. Here ε_r denotes the dielectric constant.

Fluid	σ (S/m)	ε_r	μ (Pa s)	ρ (kg/m^3)
Glycerol	7.8×10^{-2}	40	0.76	1256
Castor Oil	4×10^{-11}	4.9	0.79	970

D. Numerical scheme

An initial value for the fluctuations in the electric field, ϵ_0, is chosen from the distribution given by Eq. (5). Equations (26), (27), and (29) are solved sequentially. The details of the numerical scheme have been provided before [22,43] and are briefly reviewed here. The field and flow are assumed to be axisymmetric, which allows an analytical integration over the azimuthal direction, reducing surface integrals to line integrals over the contour of the drop. The top half of the drop is divided into N elements, creating $N + 1$ nodes. The nodes are called source points, and their coordinates are denoted by $\boldsymbol{x}$ (Fig. 1). All variables of interest are interpolated as cubic splines with respect to the arc length, s. The integral over the contour of the drop is expressed as a sum of integrals over each element. Singular terms in the integrand are subtracted out and then added back, following standard regularization techniques [44]. The integrals are evaluated using Gauss-Legendre quadrature. The points at which the integral are evaluated are referred to as observer points, and their coordinates are denoted by $\boldsymbol{y}$. After the electric field and fluid flow is calculated, the surface charge density Eq. (30) and shape of the interface Eq. (31) are updated, the latter using the second-order Runge-Kutta method, and the deformation is calculated. The fluctuation in the electric field at the next time step is then calculated from Eq. (4) using the algorithm given in Ref. [35] and is used to update the boundary value of E_∞ in Eq. (26).

The time step of the Runge-Kutta method and N are chosen to ensure that the volumetric flow rate across the interface, which should identically be zero to conserve mass, is at most $\mathcal{O}(10^{-6})$ for the initial 20 iterations. This ensures numerical stability of the computations. If the volumetric flow rate across the interface remains $\mathcal{O}(10^{-6})$ or less, while the maximum value of the radial velocity keeps on decreasing, and reaches $\mathcal{O}(10^{-4})$ or less, then we conclude that the drop has attained a steady shape. If the volumetric flow rate slowly starts to increase, along with an increase in the maximum value of the radial velocity, then we conclude that the drop shape will be unsteady, and it will result in break up. The boundary integral method cannot track the interface after the drop breaks; in this case, the results are reported at a time instant very close to breakup, where the ratio of volumetric flow rate across the interface to the initial volumetric flow rate is 100. Some computations predicted drop shapes that were not fore-aft symmetric. This occurred when the electric field fluctuated by a large magnitude in one time step, causing numerical errors. The results of these computations were discarded.

After performing one computation for the final state of the drop using a given initial value of ϵ_0, the numerical scheme is repeated for several other initial values of ϵ_0 taken from the distribution Eq. (5). The transient deformation of the drop, and the final state of the drop are reported as an average over this ensemble of initial values of ϵ_0. For this work, the computations were performed for 100 different initial values of the fluctuation in the electric field.

III. DROP DEFORMATION AND BREAKUP

We select parameter values corresponding to a drop of glycerol with 5M sodium chloride, having an initial radius $a_0 = 0.5$ mm suspended in castor oil. The physical properties of the system can be found in Ref. [21], and are listed in Table I. For this combination of fluids, the ratios of physical properties are $M = 0.96$, $S = 8.16$, and $R = 5.1 \times 10^{-10}$. Since the two fluids are nearly viscosity matched, we take $M = 1$ in the computations. At the highest electric field strength

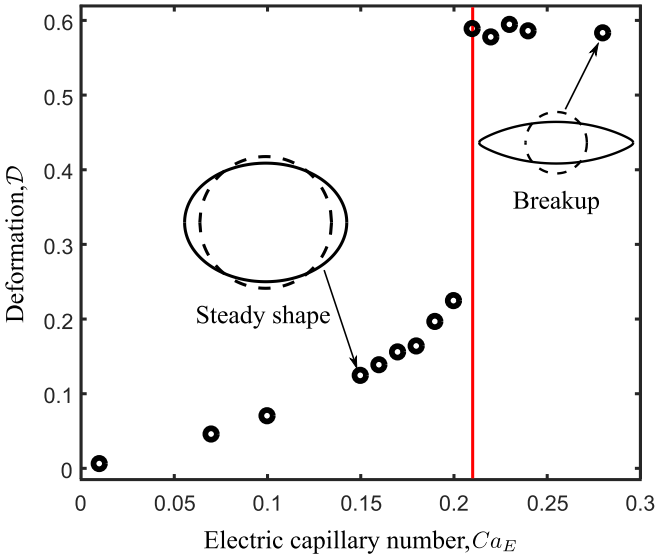

FIG. 3. Deformation plotted as a function of the electric capillary number. For drops that deform to a steady shape, the deformation corresponds to the steady final deformation. For drops that undergo breakup, the deformation corresponds to the deformation before breakup. The insets show the final shapes of a drop that reaches a steady shape, and a drop that breaks up with pointed ends. The vertical line demarcates the transition of the system from a steady final state to breakup by pointed ends. The critical electric capillary number for the transition is $\mathrm{Ca}_E \approx 0.21$.

chosen in this work, $\mathrm{Re}_i = 6 \times 10^{-3}$, $\mathrm{Re}_o = 4 \times 10^{-3}$, and for any field $\mathrm{Re}_{i,o}/\langle \mathrm{Ca}_E \rangle < 10^{-2}$. This justifies the assumptions in reducing the Navier-Stokes equation to the quasisteady Stokes equations. The assertion of quasisteady Stokes flow also means that we have (implicitly) assumed that the time scale for fluctuations in the field is large compared to the momentum diffusion time around the drop.

A. Constant electric field

We first evaluate the response of the drop to a uniform D.C. electric field. When the applied field is such that the electric capillary number $\mathrm{Ca}_E \lesssim 0.21$, the drop deforms to a steady spheroidal shape, as shown in Fig. 3. The steady deformation increases with an increase in Ca_E because of an increase in the strength of the electric stresses. At $\mathrm{Ca}_E \approx 0.21$ the electric stresses become large enough to overcome capillary stresses, and cause the drop to undergo breakup. As shown in the inset of Fig. 3, the drop breaks up with the formation of pointed ends for all $\mathrm{Ca}_E > 0.21$. This predicted critical Ca_E for breakup is similar to the values reported earlier for conducting drops [21,46]. The deformation and instability of drops is similar to the dynamics of vesicles in external fields [47–49]. However, the deformation of the drop diverges linearly as Ca_E approaches the critical value, unlike the deformation of vesicles, where the vesicle extension diverges as a power-law as the capillary number approaches a critical value [48].

B. Comparison of small deformation theory to boundary integral computations

We first predict the transient deformation of a drop under small electric fields, and compare the results from boundary integral computations to the small deformation theory. Figure 4 shows the result at a mean electric capillary number, $\langle \mathrm{Ca}_E \rangle = 0.01$, and a variance in the fluctuations, $G_w \lambda = 0.1$. The computations involve selecting an initial value for the fluctuations in the electric

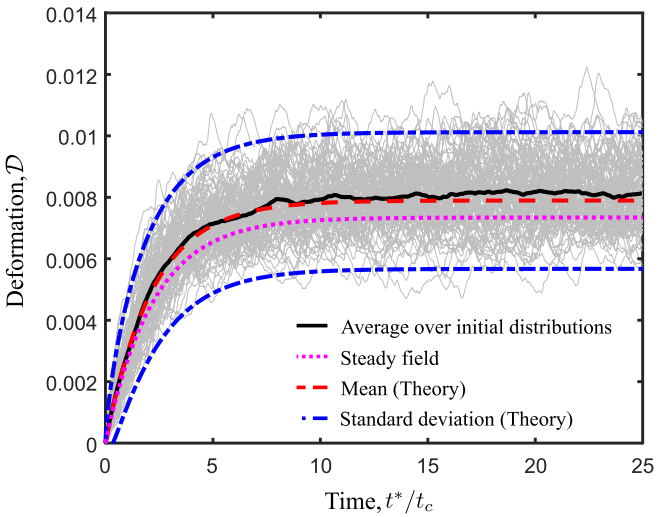

FIG. 4. Transient deformation of the drop at a mean electric capillary number $\langle \mathrm{Ca}_E \rangle = 0.01$ and variance in the fluctuations $G_w\lambda = 0.1$. The light-gray curves correspond to the transient deformation for a given initial value of the fluctuation in electric field, ϵ_0, calculated using boundary integral computations. The solid curve is calculated as the average of the gray curves, and represents the average transient deformation taken over 100 values of ϵ_0. The dashed curve corresponds to the average transient deformation, $\langle \mathcal{D}(t) \rangle$, calculated using the small deformation theory Eq. (24). The dash-dotted curves predict the deformation one standard deviation from the mean, obtained from the small deformation theory Eq. (25). The dotted curve shows the transient deformation of the drop under a steady D.C. field at $\mathrm{Ca}_E = 0.01$, predicted by boundary integral computations.

field, ϵ_0, from the distribution given by Eq. (5), and calculating the transient deformation for the chosen ϵ_0. Each light-gray curve in Fig. 4 corresponds to the computed transient deformation for a given ϵ_0. After computing the deformation for 100 different values of ϵ_0, an average is taken over the ensemble of initial distribution, and is shown by the solid curve. The mean transient deformation $\langle \mathcal{D}(t) \rangle$, predicted by the small deformation theory in Eq. (24), is shown by the dashed curve in Fig. 4. The mean deformation obtained from the boundary integral computations match the predictions of the small deformation theory. Moreover, nearly all the transient deformation curves obtained for a given ϵ_0 from the computations lie within one standard deviation from the mean predicted by the small deformation theory, shown by the dash-dotted lines in Fig. 4. This verifies that the numerical scheme we use in the computations is accurate.

For comparison, the transient deformation of the drop under a steady D.C. electric field at $\mathrm{Ca}_E = 0.01$ is shown by the dotted line in Fig. 4. Both the computations and the small deformation theory predict that the final steady deformation of the drop under a fluctuating electric field is greater than the deformation under a constant field. The small deformation theory, Eq. (24), predicts this difference in the final steady deformation to be proportional to the fluctuations in the electric field. Comparing the final steady deformation, we find that $\langle \mathcal{D}(t) \rangle - \mathcal{D}_{\mathrm{DC}} = 8 \times 10^{-4} \sim \mathcal{O}(\mathcal{D}_{\mathrm{DC}} G_w \lambda)$, as predicted by Eq. (24). This difference increases as the fluctuations grow stronger. The fluctuations increase as the variance of the underlying white noise, G_w, increases, or as the correlation time λ^{-1} decreases. A higher variance increases the spread of the electric field around the mean. A reduction in the correlation time implies that the fluctuations have less memory of their history, and can suddenly grow from values less than the mean to values greater than the mean. Hence, the probability of the drop being exposed to larger fields increases with the strength of the fluctuations. The deformation of the drop scales quadratically with the electric field, E_∞^2; hence, the net effect of the fluctuations about the mean field will not negate each other, and the mean deformation under a fluctuating field will be different from that under a constant field. The drop is exposed to fields both

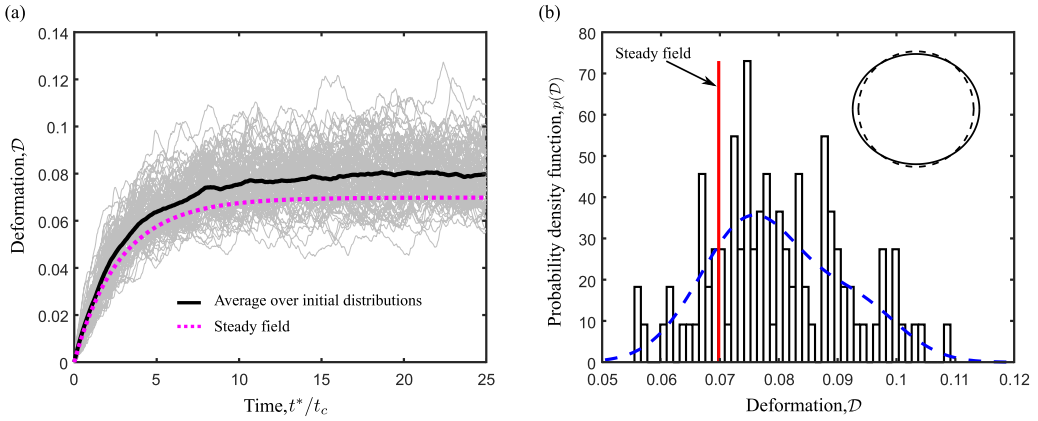

FIG. 5. (a) Transient deformation of a drop at $\langle \mathrm{Ca}_E \rangle = 0.1$ and $G_w\lambda = 0.1$. The light-gray curves correspond to the transient deformation for a given initial value of the fluctuation in electric field, ϵ_0, calculated using boundary integral computations. The solid curve is calculated as the average of the gray curves, and represents the average transient deformation taken over 100 values of ϵ_0. The dotted curve shows the transient deformation of the drop under a steady D.C. field at $\mathrm{Ca}_E = 0.1$. (b) Probability density function of the final deformation of the drop. The dashed curve is a fit of a mixture of two normal distributions to the probability density function. The solid line shows the final deformation of the drop under a steady D.C. electric field. The top-right inset shows the mean deformed steady state of the drop at $t = 25$, with the initial state shown by the dashed circle for reference.

larger and smaller than the mean field, driven by the fluctuations. On an average, the effects under the larger fields dominate, and the mean final deformation of the drop is greater than the deformation under a constant electric field. The net effect of fluctuations in the electric field is to deform a drop more than a steady D.C. field.

C. "Low" mean electric capillary number

Next we calculate the deformation of the drop at a "low" mean electric capillary number, where the small deformation theory is not valid, yet which is smaller than the critical electric capillary number for breakup under a steady field ($\mathrm{Ca}_E = 0.21$). Figure 5(a) shows the transient deformation of a drop at $\langle \mathrm{Ca}_E \rangle = 0.1$ and $G_w\lambda = 0.1$. Akin to Fig. 4, the light-gray curves correspond to computations for a given initial value of the electric field fluctuation ϵ_0, and the solid black curve represents the average transient deformation over 100 values of ϵ_0. The dotted curve shows the transient deformation under a steady D.C. electric field for $\mathrm{Ca}_E = 0.1$. The computations were performed till twice the time taken for the drop to reach steady state under a steady field. For all values of ϵ_0, the computations predict a steady deformation of the drop. Similar to the observations at small deformation, the mean deformation under a fluctuating electric field is greater than under a steady electric field. This is further shown by plotting the probability density function of the final deformation [$\mathcal{D}(t = 25)$] of the drop [Fig. 5(b)]. The deformation scales nonlinearly with the applied field, therefore the distribution function is not Gaussian. The dashed curve was obtained by fitting a mixture of two normal distributions to the final deformation, and is shown in the figure to guide the eye. Clearly, fluctuations in the electric field increase the mean deformation of the drop.

D. "High" mean electric capillary number

The system considered undergoes breakup with pointed ends at $\mathrm{Ca}_E = 0.21$ when subjected to a constant electric field. We investigate the system at $\langle \mathrm{Ca}_E \rangle = 0.28$ and $G_w\lambda = 0.1$ to determine

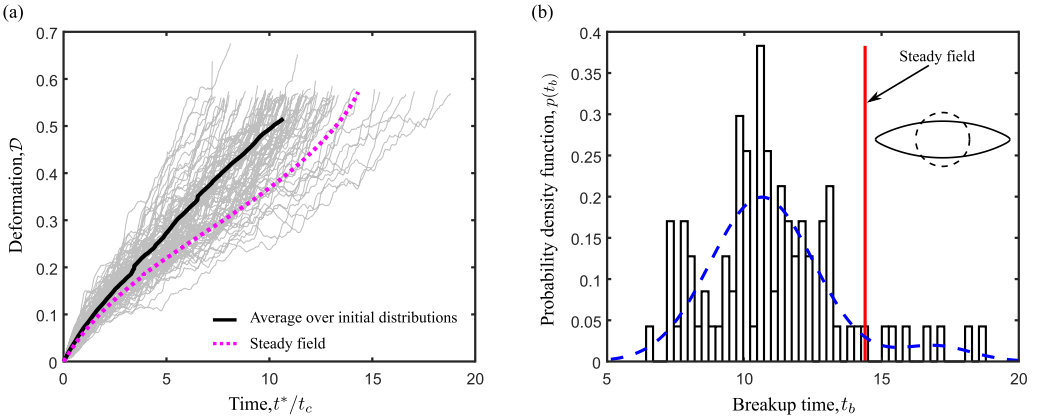

FIG. 6. (a) Transient deformation of a drop at $\langle \mathrm{Ca}_E \rangle = 0.28$ and $G_w\lambda = 0.1$. The light-gray curves correspond to the transient deformation for a given initial value of the fluctuation in electric field, ϵ_0, calculated using boundary integral computations. The solid curve is calculated as the average of the gray curves, and represents the average transient deformation taken over 100 values of ϵ_0. The dotted curve shows the transient deformation of the drop under a steady D.C. field at $\mathrm{Ca}_E = 0.1$. (b) Probability density function of the breakup time of the drop. The dashed curve is a fit of a mixture of two normal distributions to the probability density function. The solid line shows the breakup time of the drop under a steady D.C. electric field. The top-right inset shows the mean shape of the drop before breakup at the point where the solid curve in panel (a) terminates, with the initial state shown by the dashed circle for reference.

the effect of fluctuations on breakup. The transient deformation for a given ϵ_0 is shown by the light-gray curves, and the average over 100 values of ϵ_0 is shown by the solid curve in Fig. 6(a). The computations were performed till twice the breakup time for the drop under a constant field, and predict breakup with pointed ends for all values of ϵ_0. The point where the curves terminate denotes the point of breakup for a given ϵ_0. The average transient deformation curve is plotted till the mean breakup time obtained from the individual gray curves. The average deformation of the drop before breakup is greater than the deformation under a steady electric field at all given times leading to breakup. More prominently, the mean breakup time under a fluctuating electric field is less than the breakup time under a steady field, as shown by the dotted curve in Fig. 6(a). The probability density function of the breakup time is shown in Fig. 6(b), with the breakup time under a constant field shown by the solid line. The breakup time does not follow a universal distribution for different $\langle \mathrm{Ca}_E \rangle$; hence, a mixture of two normal distribution functions was fit to the probability density function and is shown by the dashed curve to guide the eye. Fluctuations in the electric field act to increase the average deformation by subjecting the drop to fields greater than the mean, which increases the rate of deformation. Although fluctuations also reduce the field from the mean value, the additional deformation due to an exposure to higher fields dominate, and consequently the drop is driven to breakup faster than under a constant field.

E. "Intermediate" mean electric capillary number

We next study the system at mean electric capillary numbers slightly less than the critical capillary number for breakup. Figure 7(a) shows the transient deformation at $\langle \mathrm{Ca}_E \rangle = 0.19$ and $G_w\lambda = 0.1$. The drop is predicted to reach a steady deformed shape under a constant electric field, the transient deformation of which is shown by the dotted curve. When the field fluctuates, there are two populations for the final state of the drop. For certain values of the initial fluctuations in the field, ϵ_0, the drop attains a deformed state at a time which is twice the time to reach steady deformation

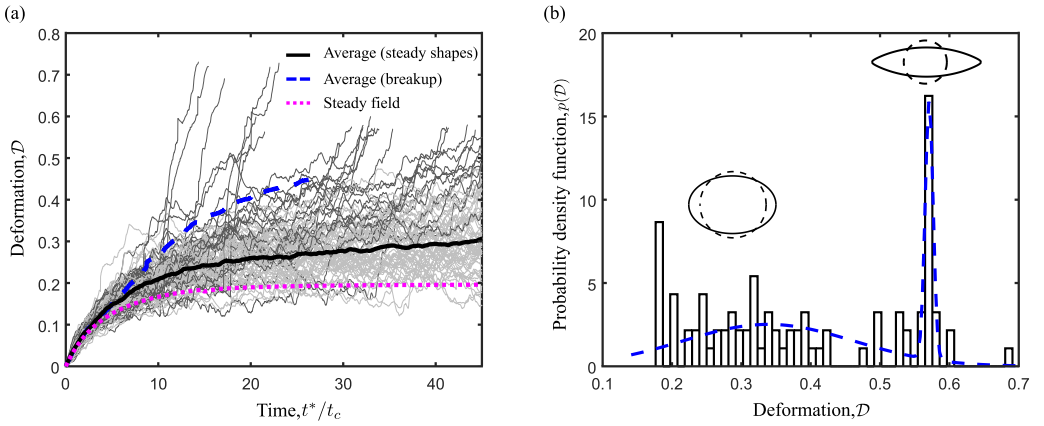

FIG. 7. (a) Transient deformation of a drop at $\langle \mathrm{Ca}_E \rangle = 0.19$ and $G_w\lambda = 0.1$ calculated using boundary integral computations. The light-gray curves correspond to the transient deformation for initial values of the fluctuation in electric field, ϵ_0, which predict steady deformation. The dark-gray curves correspond to the transient deformation for ϵ_0 values that predict breakup. The solid curve is calculated as the average of the light-gray curves, and the dashed curve is calculated as the average of the dark-gray curves. The dotted curve shows the transient deformation of the drop under a steady D.C. field at $\mathrm{Ca}_E = 0.19$. (b) Probability density function of the final deformation (for drops reaching steady state) or final deformation before breakup (for drops that undergo breakup). The dashed curve is a fit of a mixture of two normal distributions to the probability density function. The insets show the mean drop shape at steady state ($t = 45$) and just before breakup [the point where the dashed curve in panel (a) terminates], with the shape of the undeformed drop at $t = 0$ shown by the dashed circles for reference.

under a constant field. This set of drops is represented by the light-gray curves in Fig. 7(a). For other values of ϵ_0, the computations predict drop breakup by pointed ends. This set is shown by the dark-gray curves. The solid black curve represents the average over the light-gray curves, and is the average transient deformation of the population of drops that do not undergo breakup throughout the time the computations were performed. The dashed curve denotes the average transient deformation of the population of drops that breakup with pointed ends. The probability density function of the deformation of the drops is shown in Fig. 7(b). For drops that attain a steady deformed state, the deformation at $t = 45$, i.e., the time till which the computations were performed is taken, and for drops that undergo breakup, the final deformation before breakup is taken for calculating the probability distribution. The distribution is bimodal with one peak corresponding to the mean deformation of drops that maintain a stable deformed state, and another peak at the average deformation of the drops before breakup.

At intermediate values of the mean electric capillary number, fluctuations in the electric field can drive the field to values greater than the critical electric field. Depending on the amount of time the drop is subjected to these larger electric fields, it may undergo breakup, or subsequently remain stable if the fluctuations lower the field back to subcritical values. All computations under random fields were performed till a time which is twice the time for a drop to reach steady state, or twice the time to undergo breakup under a constant electric field. From Fig. 7(a) it follows that some of the drops that are predicted to attain a stable deformed state at $t = 45$ could undergo breakup if the computations were run longer, unless the electric field fluctuations eventually become less than the mean electric field. The final population of drops undergoing breakup or attaining a steady deformed shape, and the peaks of the bimodal distribution will depend on the time till which the computations are performed. The transition of the drop from a steady deformed state to a state of breakup does not occur at a distinct electric capillary number due to fluctuations in the electric field.

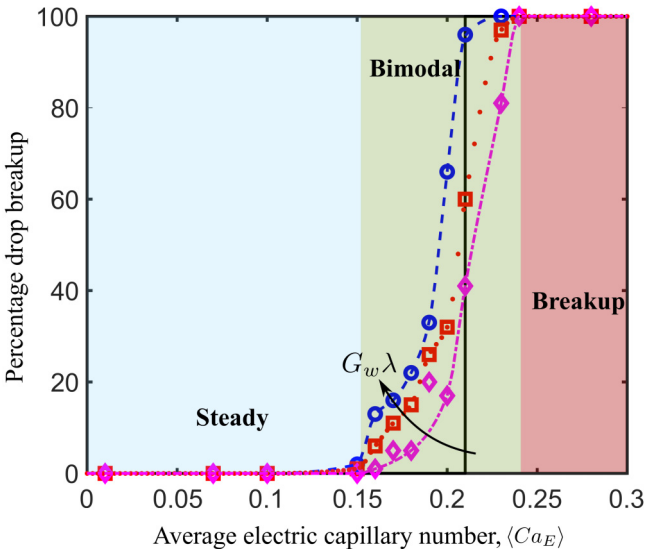

FIG. 8. Percentage of drops that undergo breakup at $t^*/t_c = 50$ as a function of the mean electric capillary number for $G_w\lambda = 0.001(\diamond)$, $0.01(\square)$, and $0.1(\circ)$. The solid curve corresponds to a steady D.C. electric field. The dashed, dotted, and dash-dotted curves are drawn to guide the eye. Based on the strength of the fluctuations and $\langle \mathrm{Ca}_E \rangle$, three final states are identified—all the drops reach steady deformation, some drops reach steady state and some undergo breakup, and all drops undergo breakup.

Droplet breakup at subcritical capillary numbers was also observed in model stochastic flow fields, and the criterion for breakup was found to depend on the transient nature of the field [29,32]. To quantify the effect of the strength of fluctuations on the transition to bimodal states and breakup, we plot the percentage of drops undergoing breakup as a function of $\langle \mathrm{Ca}_E \rangle$ for different values of $G_w\lambda$. The percentage is calculated as the fraction of the computations with a given initial fluctuation in the field (ϵ_0) predicting breakup. The result is shown in Fig. 8. When the external field is steady, characterized by $G_w\lambda = 0$, there is a sharp transition at $\langle \mathrm{Ca}_E \rangle = 0.21$ from steady deformation to drop breakup, as shown by the solid curve. Fluctuations in the electric field soften this transition by instantaneously subjecting the drop to an electric field greater than the critical value, even when the mean field is subcritical. As a result, instances of drop breakup are observed over a range of $\langle \mathrm{Ca}_E \rangle$, instead of a distinct critical $\langle \mathrm{Ca}_E \rangle = 0.21$. The mean fraction of drops that undergo breakup at a given $\langle \mathrm{Ca}_E \rangle$ and a specific time instant increases with the strength of fluctuations. Large fluctuations, quantified by a larger value of $G_w\lambda$ have a higher probability of driving the electric field to values greater than the critical for a given $\langle \mathrm{Ca}_E \rangle$, compared to weaker fluctuations. As shown in Fig. 8, at $\langle \mathrm{Ca}_E \rangle = 0.18$, 22% drops undergo breakup for $G_w\lambda = 0.1$, while 5% drops undergo breakup at the same $\langle \mathrm{Ca}_E \rangle$ when $G_w\lambda = 0.001$. When $G_w\lambda = 0.1$, all the drops were predicted to undergo breakup at $\langle \mathrm{Ca}_E \rangle > 0.21$. For weaker fluctuations, a fraction of drops are not observed to undergo breakup within the time of the computations. This fraction would eventually breakup if the computations were allowed to run longer. Weaker fluctuations are characterized by a longer correlation time, or a stronger memory of the fluctuation history. Hence, when fluctuations reduce the field to subcritical values, the field remains at those values for a longer period of time. Consequently, for the drops where this occurs, the breakup time for the individual drop would be longer. The mean breakup time for the population that breaks up is still smaller than the breakup time under constant fields. Moreover, since the mean field is greater than the critical, all the drops would eventually undergo breakup. The boundaries in Fig. 8 demarcating regions of steady deformation, bimodal distribution and drop breakup depend on the time when the system is analyzed.

IV. DISCUSSION

The response of a drop to a fluctuating electric field is remindful of shape fluctuations and conformational dynamics of vesicles [47,49,50] and the extension of polymer molecules under external flow fields [30,31,51–55]. Fluctuations in the electric field results in a larger drop deformation than under a steady electric field. The fluctuations in the drop shape are thus equivalent to a drop with a larger area. This is analogous to fluctuating membranes, where shape fluctuations arise due to thermal noise and the excess area is proportional to the temperature [50]. Under an external flow field, vesicles undergo an extension. The rate of extension of an individual vesicle is determined by the initial configuration, which is set by thermal fluctuations. Similarly, polymer molecules are stretched from an initial configuration under a flow field. The specific initial configuration of a polymer molecule, termed molecular individualism [51], is determined from a random thermal equilibration process, and dictates the rate of extension of the molecule. Akin to the rate of extension of a vesicle and a polymer molecule, the transient deformation of a drop under a random electric field follows a trajectory based on the initial random fluctuation, ϵ_0; thus, the time to reach steady state or to breakup is different for an individual drop.

The softening in transition from steady deformation to drop breakup due to increasing fluctuations in the electric field is analogous to the coil-stretch transition of polymers [30,31,51–55], and tubular to symmetric dumbbell shape transitions of vesicles under external flows [47–49]. When subjected to an external flow field, a polymer molecule gets stretched from an initial configuration. The extension of a polymer molecule depends on the strength and nature of the flow field. In a pure extensional flow, a polymer molecule exhibits a sharp transition at a critical value of the dimensionless flow strength from a coiled state, where the extension is relatively low, to a stretched state characterized by a high extension approaching the contour length. The molecule tends to align along the extensional axis of the flow, and may be driven out of this axis by Brownian motion into a coiled state. Beyond a critical value, the flow is strong enough to overcome Brownian forces and result in a stretched configuration. The addition of a rotational component to the external flow diminishes the sharpness of this transition. In addition to Brownian forces, the vorticity of the external flow can also drive the polymer away from the extensional eigenvectors of the flow into orientations where the flow exerts less stretching force, thereby reducing the sharpness in transition. Vesicle shape transitions from tubular to symmetric dumbbell shapes also show variability in the value of the critical capillary number for shape transition. In addition, the vesicle shape transition is accompanied by large fluctuations in the transient extension of an individual vesicle near the critical point, which is attributed to membrane fluctuations due to thermal noise. The fluctuations in the electric field play a role analogous to membrane fluctuations, and Brownian forces and the rotational component of the flow field, by driving the electric field to values greater than the critical field, even when the mean field is subcritical, or to values smaller than the critical field when the mean field is super-critical. As a result, the transition from exclusively steady deformation to breakup occurs gradually over a range of $\langle \mathrm{Ca}_E \rangle$.

The source of fluctuations in real systems could be the presence of multiple drops of different size at different positions with respect to the test drop, interaction with walls, or disturbances in operating conditions. The strength of the fluctuations would depend on the polydispersity of the system, concentration of drops, and the magnitude of disturbances. As such, determining operating conditions based on the response of a single drop under a well-defined external field can lead to unexpected results. For instance, in electrocoalescers, where electric fields are employed to demulsify oil-water systems, an operating electric field would be set to maximize the frequency of collision of drops, without causing breakup. The collision frequency, and the separation efficiency increases with electric field strength [56]; hence, a natural choice is to set the electric field to a large value, yet less than the critical field for breakup. We show here that fluctuations can cause certain fraction of drops to breakup even at subcritical fields, which is undesirable for coalescence. The electric capillary number scales as the square of the electric field, hence even at fields sufficiently lower than the critical, drop breakup might occur. For the system studied, drop breakup can start

at $\langle \mathrm{Ca}_E \rangle = 0.15$ depending on the strength of the fluctuations. This corresponds to a decrease in the critical electric field for breakup from 4.1 kV/cm to 3.4 kV/cm. On the contrary, the effect of fluctuations can be desirable in applications where emulsifying immiscible liquids is the goal [11]. A lower electric field can be employed to create an emulsion. Conversely, at the same electric field, the emulsification can take place faster because of the reduction in the average breakup time of drops under fluctuating fields.

In this work we have only considered the dynamics of a conducting drop to the fluctuating electric field. The behavior of leaky dielectric systems, for example an oil drop suspended in a bulk oil phase, is expected to show more novel dynamics in response to the fluctuations. The electric field inside the drop phase is finite in leaky dielectric systems. This gives rise to tangential electric stresses in addition to the normal electric stresses at the interface, which sustains a fluid flow in both the drop and medium phase fluids even when the drop deforms to a steady shape [57]. For leaky dielectric systems, the drop can deform to a prolate A shape with the fluid flow directed towards the tips of the drop, a prolate B shape where the fluid flow is away from the tips of the drop, or an oblate shape [13,20,22,58]. Similar to the transition from steady to unsteady shapes for conducting drops, the boundary demarcating prolate A, prolate B and oblate shapes for leaky dielectric drops may depend on the strength of fluctuations for a fluctuating electric field. Further, the induced electrohydrodynamic flow leads to the convection of surface charges [7,22,43,57]. Surface charge convection has been observed to cause a transition in the breakup modes of leaky dielectric drops [43]. A fluctuating electric field is likely to change the boundaries for this transition in breakup modes as well.

It should be noted that even under a fluctuating electric field, the conducting drop will not deform to oblate shapes. The formation of oblate shapes requires an electrohydrodynamic flow directed away from the tips of the drop, which is sustained due to a tangential component of the electric stresses at the interface. The electric field inside a conducting drop is zero; thus, a conducting drop does not support tangential electric stresses. The normal electric stresses ($\sim\cos^2\theta$ in small-deformation theory) is maximum at the ends of the drop and zero at the equator of the drop. Hence, the drop should always deform to a prolate shape. This can be explained mathematically in the small-deformation limit as well. For the drop to deform to a steady oblate shape under fluctuations, we must have $\langle \mathcal{D} \rangle < \sqrt{\mathrm{var}(\mathcal{D})}$ in the limit $t \to \infty$, where $\langle \mathcal{D} \rangle$ and $\mathrm{var}(\mathcal{D})$ are given by Eqs. (24) and (25), respectively. This is a quadratic equation in the variance of the electric field fluctuations, $G_w\lambda$, and has imaginary roots with a negative real part. This means that for all physically possible fluctuations ($G_w\lambda > 0$), $\langle \mathcal{D} \rangle > \sqrt{\mathrm{var}(\mathcal{D})}$, which implies that the conducting drop will deform to a prolate shape.

V. CONCLUSION

We have studied the dynamics of a conducting drop suspended in a dielectric liquid under a randomly fluctuating electric field. The transient deformation of the drop was first predicted using a small deformation theory where the mean electric capillary number is small ($\langle \mathrm{Ca}_E \rangle \ll 1$). The mean deformation and variance in deformation were predicted, and the expressions were found to match the results for drop deformation under a constant field in the limit of zero fluctuations. Nonlinear deformation and breakup were predicted using boundary integral computations, which were validated using the small deformation theory.

The random electric field is specified by its mean, which sets $\langle \mathrm{Ca}_E \rangle$, and its variance, $G_w\lambda$, which denotes the strength of fluctuations. The net effect of fluctuations at any $\langle \mathrm{Ca}_E \rangle$ is to increase the deformation of the drop compared to the deformation under a constant field. The extent of the increase in deformation depends on the strength of the fluctuations. When $\langle \mathrm{Ca}_E \rangle$ is greater than the critical electric capillary number for breakup, the increased deformation manifests as a decrease in the time taken for the drop to undergo breakup. More interestingly, at $\langle \mathrm{Ca}_E \rangle$ slightly less than the critical value, there exists two populations of drops, one that attains a steady deformed state and another that undergoes breakup. The range of $\langle \mathrm{Ca}_E \rangle$ for which this bimodal distribution is observed depends on the strength of the fluctuations.

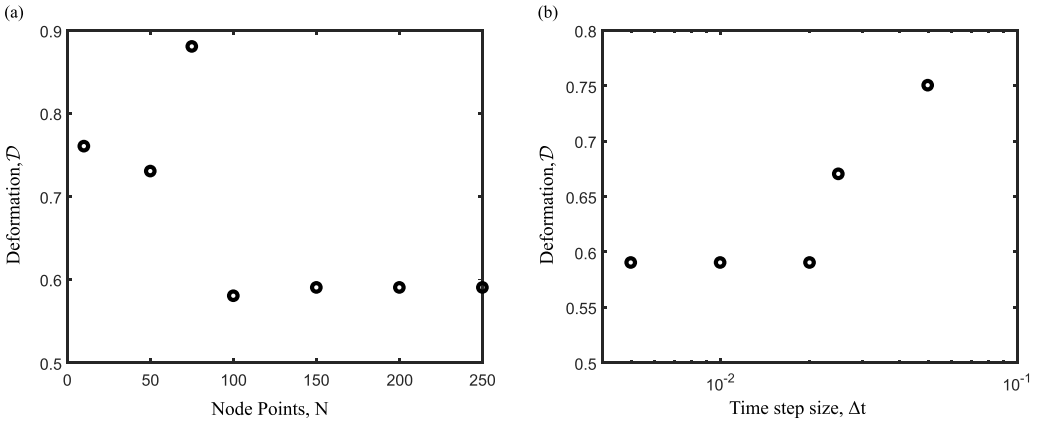

FIG. 9. Convergence results for the system under a constant electric field at $\mathrm{Ca}_E = 0.24$. Final deformation before breakup for (a) different values of N at $\Delta t = 0.02$ and (b) different values of Δt at $N = 150$.

ACKNOWLEDGMENTS

Funding for this work was provided by the National Science Foundation through Grant No. CBET-1804548. R.S. acknowledges the funding provided by the John E. Swearingen Graduate fellowship, and the Bushnell Fellowship.

APPENDIX: CONVERGENCE TESTS

Here we present a convergence analysis to select the number of nodes, N, into which the top half of the drop is partitioned, and the time step size, Δt. For the system considered here, $(M, S, R) = (1, 8.16, 5.1 \times 10^{-10})$, and the convergence tests were performed for a uniform D.C. electric field at $\mathrm{Ca}_E = 0.24$. The results are shown in Fig. 9. Increasing N beyond 150, and reducing Δt below 0.02 does not significantly change the predicted final deformation before breakup. Moreover, all the chosen N and Δt predict breakup with the formation of pointed ends, confirming that this is not a numerical artefact. In all our computations, we fixed $N = 150$ and $\Delta t = 0.02$.

[1] J. Zeleny, Instability of electrified liquid surfaces, Phys. Rev. **10**, 1 (1917).
[2] C. T. R. Wilson and G. I. Taylor, The bursting of soap bubbles in a uniform electric field, Math. Proc. Cambridge Philos. Soc. **22**, 728 (1925).
[3] W. Macky, Some investigations on the deformation and breaking of water drops in strong electric fields, Proc. R. Soc. Lond. A **133**, 565 (1931).
[4] C. T. O'Konski and H. C. Thacher Jr., The distortion of aerosol droplets by an electric field, J. Phys. Chem. **57**, 955 (1953).
[5] R. Allan and S. Mason, Particle behavior in shear and electric fields. I. Deformation and burst of fluid drops, Proc. R. Soc. Lond. A **267**, 45 (1962).
[6] G. I. Taylor, Disintegration of water drops in an electric field, Proc. R. Soc. Lond. A **280**, 383 (1964).
[7] D. Saville, Electrohydrodynamics: The Taylor-Melcher leaky dielectric model, Annu. Rev. Fluid Mech. **29**, 27 (1997).
[8] J. B. Fenn, M. Mann, C. K. Meng, S. F. Wong, and C. M. Whitehouse, Electrospray ionization for mass spectrometry of large biomolecules, Science **246**, 64 (1989).

[9] J. S. Eow, M. Ghadiri, A. O. Sharif, and T. J. Williams, Electrostatic enhancement of coalescence of water droplets in oil: A review of the current understanding, Chem. Eng. J. **84**, 173 (2001).
[10] S. Mhatre, V. Vivacqua, M. Ghadiri, A. Abdullah, M. Al-Marri, A. Hassanpour, B. Hewakandamby, B. Azzopardi, and B. Kermani, Electrostatic phase separation: A review, Chem. Eng. Res. Des. **96**, 177 (2015).
[11] T. Scott and W. Sisson, Droplet size characteristics and energy input requirements of emulsions formed using high-intensity-pulsed electric fields, Sep. Sci. Technol. **23**, 1541 (1988).
[12] R. B. Karyappa, A. V. Naik, and R. M. Thaokar, Electroemulsification in a uniform electric field, Langmuir **32**, 46 (2015).
[13] S. Torza, R. Cox, and S. Mason, Electrohydrodynamic deformation and bursts of liquid drops, Phil. Trans. R. Soc. Lond. A **269**, 295 (1971).
[14] O. Vizika and D. Saville, The electrohydrodynamic deformation of drops suspended in liquids in steady and oscillatory electric fields, J. Fluid Mech. **239**, 1 (1992).
[15] P. F. Salipante and P. M. Vlahovska, Electrohydrodynamics of drops in strong uniform dc electric fields, Phys. Fluids **22**, 112110 (2010).
[16] O. Ajayi, A note on taylor's electrohydrodynamic theory, Proc. R. Soc. Lond. A **364**, 499 (1978).
[17] J. Sherwood, Breakup of fluid droplets in electric and magnetic fields, J. Fluid Mech. **188**, 133 (1988).
[18] O. A. Basaran, T. W. Patzek, R. E. Benner Jr., and L. Scriven, Nonlinear oscillations and breakup of conducting, inviscid drops in an externally applied electric field, Ind. Engng Chem. Res. **34**, 3454 (1995).
[19] J. Q. Feng and T. C. Scott, A computational analysis of electrohydrodynamics of a leaky dielectric drop in an electric field, J. Fluid Mech. **311**, 289 (1996).
[20] E. Lac and G. Homsy, Axisymmetric deformation and stability of a viscous drop in a steady electric field, J. Fluid Mech. **590**, 239 (2007).
[21] R. B. Karyappa, S. D. Deshmukh, and R. M. Thaokar, Breakup of a conducting drop in a uniform electric field, J. Fluid Mech. **754**, 550 (2014).
[22] J. A. Lanauze, L. M. Walker, and A. S. Khair, Nonlinear electrohydrodynamics of slightly deformed oblate drops, J. Fluid Mech. **774**, 245 (2015).
[23] R. Haywood, M. Renksizbulut, and G. Raithby, Transient deformation of freely-suspended liquid droplets in electrostatic fields, AIChE J. **37**, 1305 (1991).
[24] G. Supeene, C. R. Koch, and S. Bhattacharjee, Deformation of a droplet in an electric field: Nonlinear transient response in perfect and leaky dielectric media, J. Colloid Interface Sci. **318**, 463 (2008).
[25] A. Esmaeeli and P. Sharifi, Transient electrohydrodynamics of a liquid drop, Phys. Rev. E **84**, 036308 (2011).
[26] J. A. Lanauze, L. M. Walker, and A. S. Khair, The influence of inertia and charge relaxation on electrohydrodynamic drop deformation, Phys. Fluids **25**, 112101 (2013).
[27] P. D. Berkman and R. V. Calabrese, Dispersion of viscous liquids by turbulent flow in a static mixer, AIChE J. **34**, 602 (1988).
[28] M. Tjahjadi and J. M. Ottino, Stretching and breakup of droplets in chaotic flows, J. Fluid Mech. **232**, 191 (1991).
[29] P. D. Patel, E. S. Shaqfeh, J. E. Butler, V. Cristini, J. Bławzdziewicz, and M. Loewenberg, Drop breakup in the flow through fixed fiber beds: An experimental and computational investigation, Phys. Fluids **15**, 1146 (2003).
[30] E. S. Shaqfeh and D. L. Koch, Polymer stretch in dilute fixed beds of fibres or spheres, J. Fluid Mech. **244**, 17 (1992).
[31] A. B. Mosler and E. S. Shaqfeh, The conformation change of model polymers in stochastic flow fields: Flow through fixed beds, Phys. Fluids **9**, 1222 (1997).
[32] A. B. Mosler and E. S. Shaqfeh, Drop breakup in the flow through fixed beds via stochastic simulation in model Gaussian fields, Phys. Fluids **9**, 3209 (1997).

[33] Y.-N. Young, J. Bławzdziewicz, V. Cristini, and R. Goodman, Hysteretic and chaotic dynamics of viscous drops in creeping flows with rotation, J. Fluid Mech. **607**, 209 (2008).
[34] X. Zhang, O. A. Basaran, and R. M. Wham, Theoretical prediction of electric field-enhanced coalescence of spherical drops, AIChE J. **41**, 1629 (1995).
[35] R. F. Fox, I. R. Gatland, R. Roy, and G. Vemuri, Fast, accurate algorithm for numerical simulation of exponentially correlated colored noise, Phys. Rev. A **38**, 5938 (1988).
[36] J. Melcher and G. Taylor, Electrohydrodynamics: A review of the role of interfacial shear stresses, Annu. Rev. Fluid Mech. **1**, 111 (1969).
[37] A. Donev, E. Vanden-Eijnden, A. Garcia, and J. Bell, On the accuracy of finite-volume schemes for fluctuating hydrodynamics, Commun. App. Math. Comput. Sci. **5**, 149 (2010).
[38] A. K. Bhattacharjee, K. Balakrishnan, A. L. Garcia, J. B. Bell, and A. Donev, Fluctuating hydrodynamics of multi-species reactive mixtures, J. Chem. Phys. **142**, 224107 (2015).
[39] G. Youngren and A. Acrivos, Stokes flow past a particle of arbitrary shape: A numerical method of solution, J. Fluid Mech. **69**, 377 (1975).
[40] J. Rallison, A numerical study of the deformation and burst of a viscous drop in general shear flows, J. Fluid Mech. **109**, 465 (1981).
[41] H. A. Stone and L. G. Leal, The effects of surfactants on drop deformation and breakup, J. Fluid Mech. **220**, 161 (1990).
[42] H. A. Stone, J. R. Lister, and M. P. Brenner, Drops with conical ends in electric and magnetic fields, Proc. R. Soc. London. Ser. A **455**, 329 (1999).
[43] R. Sengupta, L. M. Walker, and A. S. Khair, The role of surface charge convection in the electrohydrodynamics and breakup of prolate drops, J. Fluid Mech. **833**, 29 (2017).
[44] C. Pozrikidis, *A Practical Guide to Boundary Element Methods with the Software Library BEMLIB* (CRC Press, Boca Raton, FL, 2002).
[45] C. Pozrikidis, *Boundary Integral and Singularity Methods for Linearized Viscous Flow* (Cambridge University Press, Cambridge, 1992).
[46] N. Dubash and A. Mestel, Behaviour of a conducting drop in a highly viscous fluid subject to an electric field, J. Fluid Mech. **581**, 469 (2007).
[47] V. Kantsler, E. Segre, and V. Steinberg, Critical Dynamics of Vesicle Stretching Transition in Elongational Flow, Phys. Rev. Lett. **101**, 048101 (2008).
[48] V. Narsimhan, A. P. Spann, and E. S. Shaqfeh, The mechanism of shape instability for a vesicle in extensional flow, J. Fluid Mech. **750**, 144 (2014).
[49] D. Kumar, C. M. Richter, and C. M. Schroeder, Conformational dynamics and phase behavior of lipid vesicles in a precisely controlled extensional flow, Soft Matter **16**, 337 (2020).
[50] S. T. Milner and S. A. Safran, Dynamical fluctuations of droplet microemulsions and vesicles, Phys. Rev. A **36**, 4371 (1987).
[51] P. De Gennes, Coil-stretch transition of dilute flexible polymers under ultrahigh velocity gradients, J. Chem. Phys. **60**, 5030 (1974).
[52] J. S. Hur, E. S. G. Shaqfeh, H. P. Babcock, and S. Chu, Dynamics and configurational fluctuations of single DNA molecules in linear mixed flows, Phys. Rev. E **66**, 011915 (2002).
[53] H. P. Babcock, R. E. Teixeira, J. S. Hur, E. S. Shaqfeh, and S. Chu, Visualization of molecular fluctuations near the critical point of the coil-stretch transition in polymer elongation, Macromolecules **36**, 4544 (2003).
[54] E. S. Shaqfeh, The dynamics of single-molecule dna in flow, J. Non-Newtonian Fluid Mech. **130**, 1 (2005).
[55] S. Gerashchenko, C. Chevallard, and V. Steinberg, Single-polymer dynamics: Coil-stretch transition in a random flow, Europhys. Lett. **71**, 221 (2005).
[56] B.-Y. Kim, J. H. Moon, T.-H. Sung, S.-M. Yang, and J.-D. Kim, Demulsification of water-in-crude oil emulsions by a continuous electrostatic dehydrator, Sep. Sci. Technol. **37**, 1307 (2002).
[57] G. I. Taylor, Studies in electrohydrodynamics. I. The circulation produced in a drop by an electric field, Proc. R. Soc. Lond. A **291**, 159 (1966).
[58] P. M. Vlahovska, Electrohydrodynamics of drops and vesicles, Ann. Rev. Fluid Mech. **51**, 305 (2019).